

Article

Dehydrogenation of Surface-Oxidized Mixtures of $2\text{LiBH}_4 + \text{Al}/\text{Additives}$ (TiF_3 or CeO_2)

Juan Luis Carrillo-Bucio, Juan Rogelio Tena-García and Karina Suárez-Alcántara *

Morelia Unit of the Materials Research Institute of the National Autonomous University of Mexico, Antigua Carretera a Pátzcuaro 8701, Col. Ex Hacienda de San José de la Huerta, Morelia 58190, Michoacán, Mexico; jlcarrillo@iim.unam.mx (J.L.C.-B.); juanrogelio_tenagarcia@iim.unam.mx (J.R.T.-G.)

* Correspondence: karina_suarez@iim.unam.mx; Tel.: +52-5623-7300 (ext. 37889)

Received: 28 September 2017; Accepted: 16 November 2017; Published: 21 November 2017

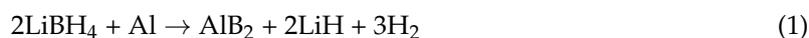
Abstract: Research for suitable hydrogen storage materials is an important ongoing subject. LiBH_4 -Al mixtures could be attractive; however, several issues must be solved. Here, the dehydrogenation reactions of surface-oxidized $2\text{LiBH}_4 + \text{Al}$ mixtures plus an additive (TiF_3 or CeO_2) at two different pressures are presented. The mixtures were produced by mechanical milling and handled under welding-grade argon. The dehydrogenation reactions were studied by means of temperature programmed desorption (TPD) at $400\text{ }^\circ\text{C}$ and at 3 or 5 bar initial hydrogen pressure. The milled and dehydrogenated materials were characterized by scanning electron microscopy (SEM), X-ray diffraction (XRD), and Fourier transformed infrared spectroscopy (FT-IR). The additives and the surface oxidation, promoted by the impurities in the welding-grade argon, induced a reduction in the dehydrogenation temperature and an increase in the reaction kinetics, as compared to pure (reported) LiBH_4 . The dehydrogenation reactions were observed to take place in two main steps, with onsets at $100\text{ }^\circ\text{C}$ and $200\text{--}300\text{ }^\circ\text{C}$. The maximum released hydrogen was 9.3 wt % in the $2\text{LiBH}_4 + \text{Al}/\text{TiF}_3$ material, and 7.9 wt % in the $2\text{LiBH}_4 + \text{Al}/\text{CeO}_2$ material. Formation of CeB_6 after dehydrogenation of $2\text{LiBH}_4 + \text{Al}/\text{CeO}_2$ was confirmed.

Keywords: hydrogen storage; borohydrides; reactive mixtures

1. Introduction

LiBH_4 is an outstanding material regarding its hydrogen content (18.4 wt %) [1]. However, its dehydrogenation temperature is too high for any practical application in hydrogen storage. Pure LiBH_4 presents two dehydrogenation steps; one minor at approximately $320\text{ }^\circ\text{C}$ and the main one at $500\text{ }^\circ\text{C}$ [1]. To reduce the dehydrogenation temperature, improve reaction kinetics or reversibility, LiBH_4 has been mixed with several compounds in different proportions. The list includes but is not limited to other borohydrides such as: $\text{Ca}(\text{BH}_4)_2$ [2], NaBH_4 [3], or $\text{Mg}(\text{BH}_4)_2$ [4], other complex hydrides such as LiNH_2 [5], alanates of Li or Na [6,7], binary hydrides such as MgH_2 [8–10], CaH_2 [11–13], TiH_2 [12], halide salts such as LiCl [14], oxides [15], scaffolds [16], and metals such as Mg, Ti, V, Cr, Sc, or Al [12,17]. The main characteristics of these mixtures are collated in Table 1.

The last system, the $2\text{LiBH}_4 + \text{Al}$, is of potential interest. Siegel et al. [18] anticipated, based on first-principles calculations, that the reaction:



would release 8.6 wt % hydrogen at $277\text{ }^\circ\text{C}$ and $p(\text{H}_2) = 1$ bar. Experimentally, Zhang et al. performed the dehydrogenation of $2\text{LiBH}_4 + \text{Al}$ at a pressure of 0.001 bar H_2 and from roughly $325\text{--}525\text{ }^\circ\text{C}$ [19]. Zhang et al. demonstrated a hydrogen release of approximately 4 wt % by means of isothermal dehydrogenation at $375\text{ }^\circ\text{C}$, meanwhile complete dehydrogenation was obtained up to $577\text{ }^\circ\text{C}$ by means

of thermogravimetric measurement [19]. Kang et al. achieved the release of 7.2 wt % hydrogen when the mixture was catalyzed with TiF_3 , at a pressure of 0.001 bar, 450 °C, and 3 h [20]. Hansen et al. [17] demonstrated that the dehydrogenation reaction of $2\text{LiBH}_4 + 3\text{Al}$ occurs at $p(\text{H}_2) = 10^{-2}$ bar when the material is heated up to 500 °C; and that the re-hydrogenation demonstrated only partial reversibility. Other examples include the experiments of Ravnsbaek et al., where the dehydrogenation reaction of $\text{LiBH}_4 + \text{Al}$ (1:0.5) was characterized by in-situ synchrotron radiation powder X-ray diffraction from room temperature to 500 °C and dynamic vacuum [21]. All these experiments have in common a very low or vacuum dehydrogenation pressure (summarized in Table 1). The vacuum dehydrogenation pressure is inadequate for any practical application. Additionally, it is well-known that the hydrogen pressure can affect the dehydrogenation products of LiBH_4 mixtures. For example with the system $2\text{LiBH}_4 + \text{MgH}_2 \rightarrow 2\text{LiH} + \text{MgB}_2 + 4\text{H}_2$, a correlation was demonstrated between the dehydrogenation pressure and re-hydrogenation [22]. With the 2LiBH_4 -Al system, Yang et al. proposed that a desorption backpressure of 3 bar could contribute to the formation of AlB_2 [12]; which would improve, in principle, the reversibility of hydrogenation/dehydrogenation reactions. A study of the dehydrogenation backpressure with 2LiBH_4 -Al systems has been poorly explored.

Among the additives for improving reaction kinetics or reversibility; TiF_3 is the material most commonly used, and it is almost mandatory to test TiF_3 in all new mixtures. In their part, oxides such as TiO_2 , ZrO_2 , Nb_2O_5 or MoO_3 have resulted in successful accelerators for hydrogen desorption reactions [23,24]. CeO_2 is not a commonly used additive for hydrogenation/dehydrogenation reactions. However, interactions of hydrogen with CeO_2 have been reported [25]. The possible effects of CeO_2 as an additive for hydrogen storage materials deserve research.

Conventionally, hydrogen storage materials are produced and handled in a high or ultra-high purity inert atmosphere, i.e., high-purity argon. This is done to avoid the deactivation of materials caused by the formation of thick oxide films that impede hydrogen diffusion from/to the bulk of the storage material. However, some reports have expressed that the use of high-purity inert atmosphere can be relaxed [26] and that allowing some surface oxidation can be helpful to the dehydrogenation kinetics [27].

Here, the dehydrogenation behavior is presented of $2\text{LiBH}_4 + \text{Al}$ added with 5 wt % of TiF_3 or CeO_2 , and surface-modified (oxidized) by the effects of impurities in welding-grade argon. The dehydrogenation reactions were performed at 3 bar and 5 bar of hydrogen. The effects of the borohydride-Al mixture, additives, and surface-oxide effects are discussed.

Table 1. Reported hydrogen desorption conditions for several LiBH_4 mixtures.

Material and/or Proposed Reaction, and Reported ΔH^0 (If Available) (kJ/mol H_2)	Desorption Conditions p (bar) and T (°C)	Comments
$\text{LiBH}_4 \rightarrow \text{LiH} + \text{B} + 3/2\text{H}_2$ [1]	p : not specified T : 320 °C and 500 °C	Multi-step dehydrogenation reaction
$\text{LiBH}_4 \rightarrow \text{Li} + \text{B} + 2\text{H}_2$ 95.1 kJ/mol H_2 [28]	p : 1 bar T : 25 °C	From standard formation enthalpy of LiBH_4
$x\text{LiBH}_4 + (1-x)\text{Ca}(\text{BH}_4)_2$ [2]	p : not specified T : 370 °C for $x = 0.4$	$x = 0 - 1$, eutectic melting at 200 °C
$0.62\text{LiBH}_4 - 0.38\text{NaBH}_4$ [3]	p : not specified T : onset at 287 °C, peaks at 488 °C and 540 °C	Multi-step dehydrogenation reaction
$x\text{LiBH}_4 + (1-x)\text{Mg}(\text{BH}_4)_2$ [4]	p : 5 bar T : 170 °C and 215 °C	$x = 0 - 1$, eutectic melting at 180 °C Multi-step dehydrogenation reaction
$\text{LiBH}_4 + 2\text{LiNH}_2 \rightarrow \text{Li}_3\text{BN}_2 + 4\text{H}_2$ 23 kJ/mol H_2 [5]	p : 100–0.01 bar T : 430 °C	From pressure composition isotherm.
$\text{LiBH}_4 + \text{LiAlH}_4$ [6]	p : 0.2 bar T : 118 °C and 210 °C	2:1 mixture, two-step dehydrogenation. Dehydrogenation temperature reduced if TiF_3 addition.
$\text{LiBH}_4 + \text{NaAlH}_4$ [7]	p : 1 bar He T : from room temperature up to 210 °C for the doped systems and 110–250 °C for the undoped systems.	Molar ratios 1:1, 2:3 and 1:3; with and without TiCl_3 additive. Multi-step dehydrogenation reaction.

Table 1. Cont.

Material and/or Proposed Reaction, and Reported ΔH^0 (If Available) (kJ/mol H ₂)	Desorption Conditions p (bar) and T (°C)	Comments
$2\text{LiBH}_4 + \text{MgH}_2 \rightarrow 2\text{LiH} + \text{MgB}_2 + 4\text{H}_2$ 50.4 kJ/mol H ₂ [10]	p : 3 bar H ₂ T : 350–400 °C	Multi-step dehydrogenation reaction
$6\text{LiBH}_4 + \text{CaH}_2 \leftrightarrow 6\text{LiH} + \text{CaB}_6 + 10\text{H}_2$ 59 kJ/mol H ₂ [11]	p : 1.3 bar flowing He T : onset at 150 °C, maximum at 350 °C, finished at 450 °C	-
$\text{LiBH}_4 + \text{TiH}_2$ [12]	p : not specified (argon) T : ~410 °C	-
$\text{LiBH}_4 + \text{LiCl}$ (1:1) to give $\text{Li}(\text{BH}_4)_{1-x}\text{Cl}_x$ ($x \approx 0.23$) [14]	p : not specified (argon) T : 300–550 °C	Cl^- to BH_4^- substitution at LiBH_4
	277 °C [18]	Theoretical desorption temperature
$2\text{LiBH}_4 + \text{Al} \rightarrow 2\text{LiH} + \text{AlB}_2 + 3\text{H}_2$ 57.9 kJ/mol H ₂ [18]	Dehydrogenation: p : 0.001 bar H ₂ T : 325 °C to 525 °C [19]	H ₂ release of about 4 wt % Multi-step dehydrogenation reaction
	p : 0.001 bar T : 450 °C [20]	Catalyzed with TiF_3
	p : dynamic vacuum T : up to 500 °C [21]	Formation of $\text{Li}_x\text{Al}_{1-x}\text{B}_2$

2. Results

2.1. Characterization of As-Milled Materials

Scanning Electron Microscopy. Some of the descriptions below contain remarks about SEM images that are shown in the Supplementary Materials. Also for comparison purposes, the SEM images of LiBH_4 and Al without milling are presented in the Supplementary Materials. Non-milled LiBH_4 is composed of large crystals embedded in an amorphous phase. Non-milled Al is composed of particles of approximately 50 μm , heavily agglomerated and forming flakes of 1 mm (Supplementary Materials). Figure 1 presents the most representative SEM images of the as-milled materials. The as-milled $2\text{LiBH}_4 + \text{Al}$ material, Figure 1a, formed a three-dimensional, porous structure. Interestingly the surface of $2\text{LiBH}_4 + \text{Al}$ is covered with crystals of approximately 2–3 μm . The material $2\text{LiBH}_4 + \text{Al}/\text{TiF}_3$, Figure 1b, also presented a three-dimensional structure. The material consisted of elongated crystals of 10 μm length and 2 μm width. Elemental analysis by energy-dispersive X-ray spectroscopy (EDS) of those crystals revealed a B-rich phase, i.e., the LiBH_4 . The addition of CeO_2 , Figure 1c, to the base material, produced an agglomerated, spherical, and compacted material of about 50 μm in diameter, with some surface formations approximating flake-shape. Here, spots of CeO_2 are clearly distinguishable from the base material. In principle, the morphology characteristics of hydrogen storage materials must be reduced particle size, low agglomeration, homogeneity of component materials, and the formation of porous structures allowing the inflow/outflow of hydrogen while maintaining good thermal conductivity. SEM images showed interesting morphologies of the $\text{LiBH}_4 + \text{Al}/\text{additives}$, depending on the additive material.

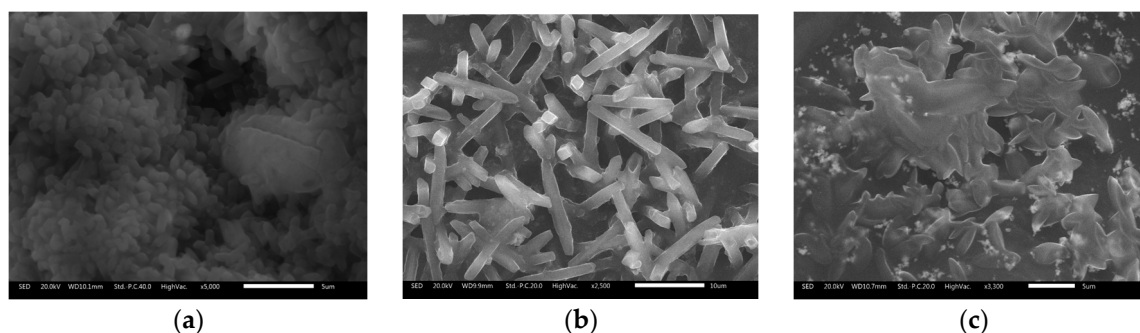


Figure 1. Scanning electron microscopy (SEM) images of the as-milled materials: (a) $2\text{LiBH}_4 + \text{Al}$; (b) $2\text{LiBH}_4 + \text{Al}/\text{TiF}_3$; (c) $2\text{LiBH}_4 + \text{Al}/\text{CeO}_2$.

Powder X-ray diffraction. Figure 2 shows the X-ray diffraction patterns of as-milled materials. In the three studied materials, the presence of Al is evidenced by the strong diffraction peaks. By contrast, the LiBH_4 presented attenuated peaks as as-milled materials. LiBH_4 diffraction peaks in Figure 2 are a mixture of orthorhombic (main) and hexagonal (minor) phases to a different degree in the different mixtures. The material $2\text{LiBH}_4 + \text{Al}/\text{CeO}_2$ presented strong peaks of CeO_2 , in agreement with the CeO_2 particles found in the SEM images. The material added with TiF_3 did not present the characteristic peaks of TiF_3 . Some researchers have proposed the in-situ formation of $\text{Ti}(\text{BH}_4)_3$ by the reaction of LiBH_4 and TiF_3 , followed by a rapid decomposition of $\text{Ti}(\text{BH}_4)_3$ [29]. Reactions to form other stable fluorine salts such as TiF_2 or AlF_3 cannot be discarded. These side reactions during ball-milling can be the reason for the absence of TiF_3 diffraction peaks. The materials also presented a small amount of aluminum oxide. Refinement of the Al and CeO_2 phases (not including LiBH_4 phases, $R_{\text{wp}} \approx 7$) produced the following Al-crystal sizes: Al in $2\text{LiBH}_4 + \text{Al}$: 309.6 ± 16.7 nm; Al in $2\text{LiBH}_4 + \text{Al}/\text{TiF}_3$: 129.0 ± 5.0 nm; Al in $2\text{LiBH}_4 + \text{Al}/\text{CeO}_2$: 142.8 ± 9.2 nm. The CeO_2 crystal size was determined as 120.3 ± 4.2 nm. All these facts point to the formation of fine mixtures of $2\text{LiBH}_4 + \text{Al}/\text{additive}$ and an influence of the additives on the crystalline characteristics of the samples.

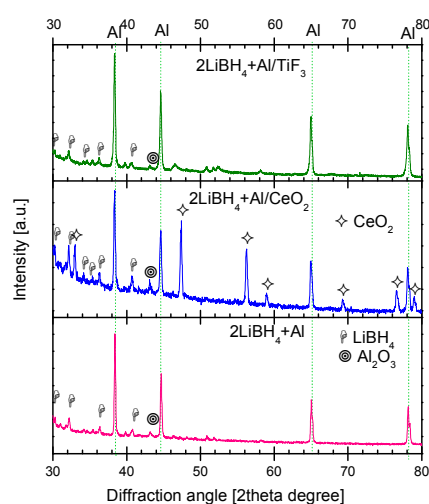


Figure 2. X-ray diffraction patterns of the as-milled materials: (a) $2\text{LiBH}_4 + \text{Al}$; (b) $2\text{LiBH}_4 + \text{Al}/\text{TiF}_3$; (c) $2\text{LiBH}_4 + \text{Al}/\text{CeO}_2$.

Fourier Transformed Infrared Spectroscopy. An effect of the ball milling is the increase of the local pressure and temperature during ball-ball or ball-vial collisions that induce the decomposition of sensitive materials. In the case of the $2\text{LiBH}_4 + \text{Al}$ mixtures, it is intended to decrease the decomposition temperature during dehydrogenation, but not to decompose during ball-milling. Thus FT-IR was performed to check the “survival” of LiBH_4 after ball-milling. Borohydrides present two regions of interest B–H bending ($1000\text{--}1600\text{ cm}^{-1}$) and H–B–H stretching ($2000\text{--}2500\text{ cm}^{-1}$) [29,30]. Both IR active modes are presented in all the as-milled samples (Supplementary Materials), indicating sufficient thermal stability during ball milling.

X-ray photoelectron spectroscopy. XPS results are presented in Figure 3. Frame 3a presents the Li 1s XPS spectra. The Li 1s XPS spectrum of LiBH_4 with a clean surface was reported to present a peak at 57.1 eV; meanwhile, the oxygen-exposed samples presented a contribution (shoulder) of Li_2O at 55.5 eV [27]. The studied materials present the main peak in a range between 57.2 and 57.5 eV. Because of that, the main contribution of Li binding is not the Li–O interactions. Frame 3(b) presents the B 1s XPS spectra. The reported peak for pure LiBH_4 is located at 188.3–188.4 eV [31]. After exposing LiBH_4 to oxygen or moisture, a new peak located at 191.5–191.4 eV emerged and it was attributed to LiBO_2 [31]. The studied materials presented both peaks, the LiBH_4 and the LiBO_2 at 188.3–188.0 eV and 191.9–191.3 eV, respectively. The peak intensity ratio of the LiBH_4 and LiBO_2 is not homogeneous

throughout the set of studied materials. The mixture of $2\text{LiBH}_4 + \text{Al}$ presented the lowest intensity of the LiBO_2 peak. Frame c of Figure 3 presents the O 1s XPS spectra; as a reference, the O 1s spectra at the Al raw-material was included. In that spectrum, the peak at 533.6 eV can be related to an Al_2O_3 layer [32]. The XPS spectra of LiBH_4 , $2\text{LiBH}_4 + \text{Al}/\text{TiF}_3$, and $2\text{LiBH}_4 + \text{Al}/\text{CeO}_2$ presented two main peaks; one at 533.9 eV and other at 532.6 eV. This last peak can be attributed to the LiBO_2 [32]. The LiBO_2 peak is very much attenuated in the $2\text{LiBH}_4 + \text{Al}$, in agreement with the result at the B 1s spectra. The Al 2p spectrum of the as-received Al and as-milled $2\text{LiBH}_4 + \text{Al}$ /additive materials is shown in the Supplementary Materials. The (as-received) Al curve presents the characteristic metallic and oxide peaks of Al [33]. Meanwhile, no signal above noise was detected for the mixtures, indicating Al segregation to sub-surface layers.

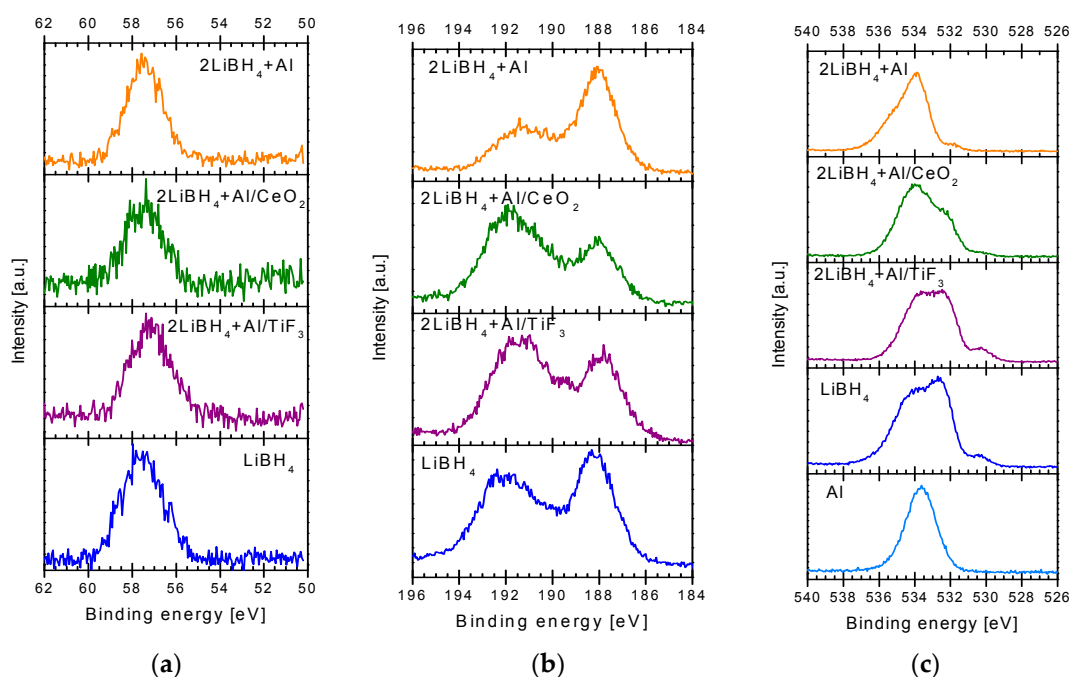


Figure 3. X-ray photoelectron spectroscopy (XPS) spectra of as-milled $2\text{LiBH}_4 + \text{Al}$, $2\text{LiBH}_4 + \text{Al}/\text{TiF}_3$, and $2\text{LiBH}_4 + \text{Al}/\text{CeO}_2$. (a) Li 1s edge; (b) B 1s edge; (c) O 1s edge.

2.2. Dehydrogenation Reactions

Figure 4 presents the dehydrogenating reactions traced by thermal-programmed control. For two frames, the sample temperature also was plotted. The dehydrogenations of $2\text{LiBH}_4 + \text{Al}$ and $2\text{LiBH}_4 + \text{Al}/\text{TiF}_3$ at 3 bar and 5 bar initial pressure are presented in Figure 4a. The dehydrogenations were performed up to 400 °C. The dehydrogenations occurred as multiple-step reactions. The first step with both materials was observed to start at 110 °C and produced a small hydrogen release. In the $2\text{LiBH}_4 + \text{Al}$ material, the second step was observed at 210 °C, and a slight change in reaction rate at roughly 325 °C. The dehydrogenation reactions in the $2\text{LiBH}_4 + \text{Al}$ material were essentially finished at 400 °C and reached a hydrogen release of -5.8 wt % for the 3 bar initial pressure reaction and -6.0 wt % for the 5 bar initial pressure reaction. The dehydrogenations of $2\text{LiBH}_4 + \text{Al}/\text{TiF}_3$ at 3 bar and 5 bar initial pressure also are multiple-step reactions. At both initial pressures, the dehydrogenation first step onset is situated at about 110 °C. At the 3 bar dehydrogenation, the second reaction step is located at 240 °C. The last step initiated at 340 °C, after a clear-defined plateau. At 3 bar initial pressure the release of hydrogen accounted for -9.3 wt %. The situation is very different for the same material at 5 bar initial pressure, here the onset of the second dehydrogenation step was observed at 200 °C. A slowdown of the dehydrogenation rate was observed at 300 °C. Finally, the dehydrogenation finished after reaching 400 °C, releasing -6.0 wt %. This last quantity is greater than the theoretical value of -8.6 wt %, thus

a release of B-compounds is probable. It means that higher initial pressure in combination with lower final temperature needs to be explored for this material.

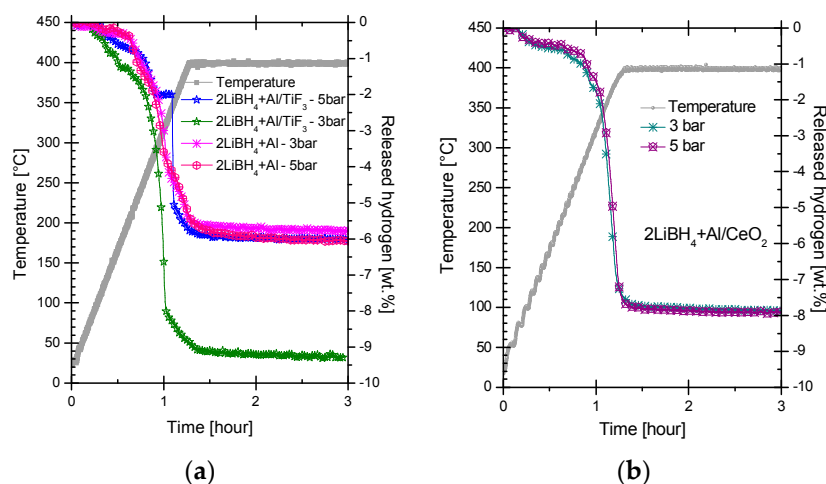


Figure 4. Temperature programmed hydrogen desorption of (a) $2\text{LiBH}_4 + \text{Al}$, and $2\text{LiBH}_4 + \text{Al}/\text{TiF}_3$; (b) $2\text{LiBH}_4 + \text{Al}/\text{CeO}_2$ at 3 and 5 bar initial pressure of hydrogen.

Figure 4b presents the dehydrogenation reactions of $2\text{LiBH}_4 + \text{Al}/\text{CeO}_2$ at 3 bar and 5 bar initial hydrogen pressure up to $400\text{ }^\circ\text{C}$. The dehydrogenation reactions are similar at both pressures and they are also multistep reactions. The onset temperature of the first dehydrogenation step is below $100\text{ }^\circ\text{C}$. The dehydrogenation reactions presented the second step starting at $220\text{ }^\circ\text{C}$. The material $2\text{LiBH}_4 + \text{Al}/\text{CeO}_2$ released $-7.9\text{ wt.}\%$ of hydrogen in both cases. In the material $2\text{LiBH}_4 + \text{Al}/\text{CeO}_2$, dehydrogenation at $350\text{ }^\circ\text{C}$ was achieved and can be observed in the Supplementary Materials. The dehydrogenation is a multi-step reaction with a hydrogen release of $-5.6\text{ wt.}\%$ at 5 bar and $-6.5\text{ wt.}\%$ at 3 bar after 3 h of reaction.

2.3. Characterization of Dehydrogenated Materials

Figure 5 presents the most representative SEM images of the $2\text{LiBH}_4 + \text{Al}$, $2\text{LiBH}_4 + \text{Al}/\text{TiF}_3$, and $2\text{LiBH}_4 + \text{Al}/\text{CeO}_2$ materials dehydrogenated at 5 bar, other SEM images are available in the Supplementary Materials. In general, dehydrogenated materials presented important agglomerations of about $200\text{ }\mu\text{m}$ size. Thus an important increase in particle size after dehydrogenation was observed. The agglomerated materials were composed of an amorphous matrix with crystalline zones of cubic or hexagonal morphologies. Elemental analysis of those crystals revealed the presence of B and Al as major components; and Ti, F, Ce, and O as minor components, accordingly with the additive. An important observation is that the atomic composition of Al and B in the crystals of all the tested materials was not consistent. The elemental analysis was performed in small areas on the crystals, and the results range from roughly the expected 1:2 atomic ratio of AlB_2 to 1:12 atomic ratio of AlB_{12} . The loss of available B for the re-hydrogenation reaction is a common drawback for all borohydrides and their mixtures. B can be lost as borane compounds (BH_3 , B_2H_6 , etc.), form B-clusters or other boranes that are unreactive at moderate pressures and temperature for further re-hydrogenation reaction. Elemental analysis during SEM data collection indicates good B retention with the dehydrogenated samples.

Due to the detection limit of elemental analysis with the SEM microscope, Li-compounds were not located. The SEM images of the materials with CeO_2 deserve some attention; the as-milled materials presented clear CeO_2 bright spots (Figure 1c); meanwhile, the dehydrogenated materials (Supplementary Materials) presented a more homogeneous distribution of Ce along the sample image. Another interesting point was a tendency to formation of crystals with higher dehydrogenation

pressure. A greater quantity of crystals was observed at samples dehydrogenated at 5 bar initial pressure than at 3 bar initial pressure.

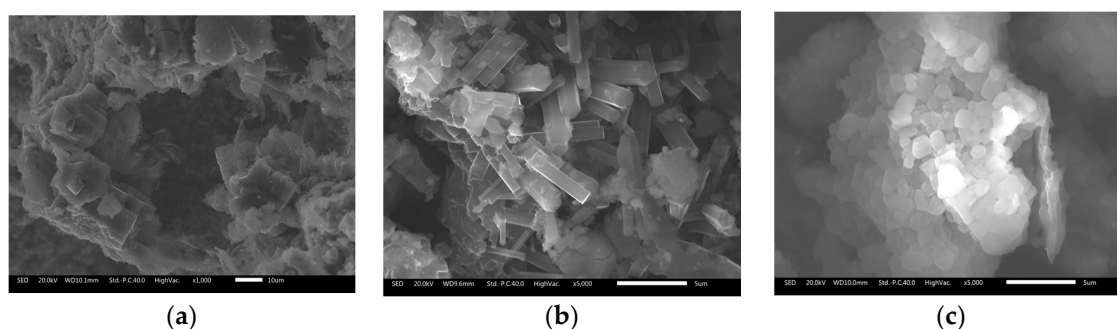


Figure 5. SEM images of the dehydrogenated (DHH) materials: (a) $2\text{LiBH}_4 + \text{Al}$ -DHH 5 bar, $400\text{ }^\circ\text{C}$; (b) $2\text{LiBH}_4 + \text{Al}/\text{TiF}_3$ -DHH 5 bar, $400\text{ }^\circ\text{C}$; (c) $2\text{LiBH}_4 + \text{Al}/\text{CeO}_2$ -DHH 5 bar, $400\text{ }^\circ\text{C}$.

Powder X-ray diffraction patterns of the dehydrogenated (labeled as DHH) materials are presented in Figure 6. The diffractograms of the dehydrogenated materials at 3, and 5 bar are presented in Frame (a,b) respectively. In general, the exact determination of the reaction extent based purely on the X-ray diffraction (XRD) results is difficult: this is due to Al and LiH sharing the same crystal symmetry and close crystal cell dimensions. Thus the peaks of the reactant and the reaction product overlap, particularly at low diffraction angles. Additionally, the (101) peak of AlB_2 (P6MMM) is pretty close to the Al (200) and LiH (200) peak, these peaks also overlap. The rest of the AlB_2 peaks are appreciable when zooming the plot with data-processing software; otherwise, these peaks appear rather small. All the dehydrogenated materials presented minor peaks of Li_2O and LiOH . The dehydrogenated $2\text{LiBH}_4 + \text{Al}$ and $2\text{LiBH}_4 + \text{Al}/\text{TiF}_3$ presented Al_2O_3 . The oxides and hydroxide could evolve/crystallize from the initial surface oxides present in the as-milled materials and the hydrogen atmosphere during heating. The dehydrogenated 3 bar- and 5 bar- $2\text{LiBH}_4 + \text{Al}/\text{CeO}_2$ materials are very interesting regarding the oxides content; they no longer present peaks of CeO_2 after the dehydrogenation reaction. CeO_2 reacted to form CeB_6 (COD-5910033).

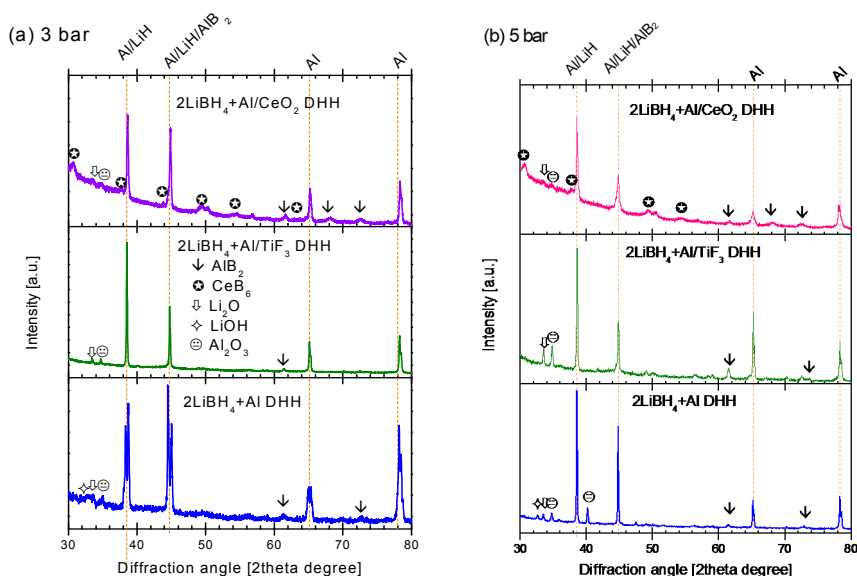


Figure 6. X-ray diffraction patterns of dehydrogenated materials. Frame (a) after dehydrogenation at 3 bar initial hydrogen pressure; Frame (b) after dehydrogenation at 5 bar initial hydrogen pressure.

FT-IR spectra of all dehydrogenated products are presented in Figure 7. This figure confirms the incomplete dehydrogenation of the materials after reactions. The dehydrogenated materials presented differences in the H–B–H bending region compared to the as-milled materials. First, a shift of the peaks to higher wavenumbers was observed, from 1100–1200 cm^{-1} in as-milled materials to 1400–1560 cm^{-1} in dehydrogenated materials. Secondly, the intensity of these peaks was different with the additive; the $2\text{LiBH}_4 + \text{Al}$ material presented the highest peak intensity meanwhile the materials added with TiF_3 and CeO_2 presented reduced signal intensity. The B–H stretching region (2000–2500 cm^{-1}) also presented shifts in wavenumber, however, this shift was not as marked as the H–B–H region. It amounts to approximately 75 cm^{-1} . The materials dehydrogenated at 5 bar presented more intense H–B–H peaks than the materials dehydrogenated at 3 bar. This result points to a different reaction mechanism.

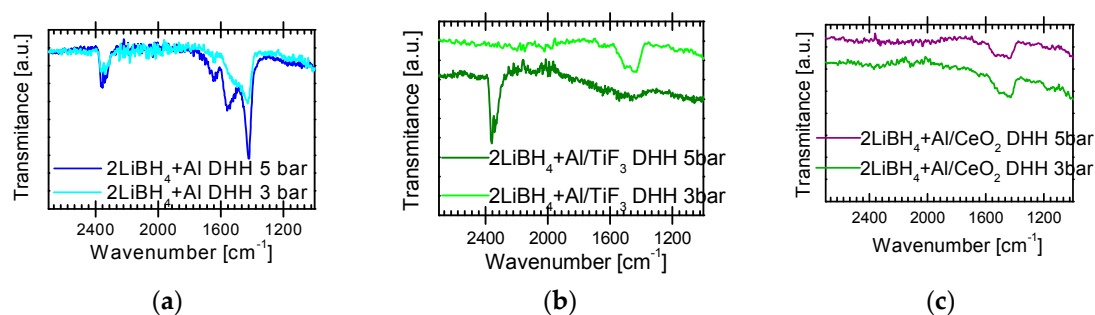


Figure 7. Fourier Transformed Infrared Spectroscopy (FT-IR) of dehydrogenated (DHH) samples: (a) $2\text{LiBH}_4 + \text{Al}$ -DHH; (b) $2\text{LiBH}_4 + \text{Al}/\text{TiF}_3$; (c) $2\text{LiBH}_4 + \text{Al}/\text{CeO}_2$ -DHH.

3. Discussion

Milling effects. A proper integration of LiBH_4 and Al in the mixtures was observed after the ball-milling. The milling of Al is not an easy process. Al has the tendency of sintering instead of dispersing unless using proper milling conditions [34]. The milling conditions used here represent a good balance between the optimum milling of Al and reduced degradation of LiBH_4 .

Protective atmosphere effects. Customarily; the storage, production, processing, and handling of hydrogen storage materials are performed with a high purity argon atmosphere, with oxygen and moisture levels below 0.1 ppm. This would raise significantly the cost of the hydrogen storage materials if commercialization is intended. In our experiments the argon purity was not so high, the supplier-guaranteed oxygen and moisture levels were 10 ppm. This allowed surface oxidation as demonstrated by means of XPS experiments. Kato et al. [27] demonstrated that the surface oxidation of LiBH_4 produces Li surface segregation, the formation of Li_2O over LiBH_4 , reduction of diborane desorption, and enhancement of the rate of hydrogen desorption. XPS suggests the formation of LiBO_2 rather than Li_2O on the surface of our samples and the segregation of Al to sub-surface layers. As a result of the surface oxidation, a reduction of the dehydrogenation temperature was observed here and compared with similar materials carefully protected against surface oxidation [17–22]. A reduction of the dehydrogenation activation barrier was proposed by Kang et al. [35] if LiBH_4 or the intermediate LiBH donate one electron (each), to a catalyst on their surfaces. Oxygen is well-known as an electron acceptor. Thus surface oxidation could reduce the activation barrier and help to reach thermodynamic-predicted temperatures for the dehydrogenation reaction.

Dehydrogenation kinetics. The dehydrogenations of the $2\text{LiBH}_4 + \text{Al}$, $2\text{LiBH}_4 + \text{Al}/\text{TiF}_3$, and $2\text{LiBH}_4 + \text{Al}/\text{CeO}_2$ materials are multi-step reactions. The multistep nature of the dehydrogenation reaction of the $2\text{LiBH}_4 + \text{Al}$ is shared with the dehydrogenation of LiBH_4 [36] and the RHC $\text{LiBH}_4 + \text{MgH}_2$ [22,37]. Reports of LiBH_4 -Al dehydrogenation in several molar proportions also described a multistep mechanism for the dehydrogenation reaction [17,19–21,38]. In the materials presented here, the first dehydrogenation step occurred at low temperature, i.e., 100–110 $^\circ\text{C}$. And the main

dehydrogenation step occurred between 200–300 °C, finishing at 400 °C. The main dehydrogenation temperature interval is close to the temperature predicted by Siegel et al. for the dehydrogenation reaction of $2\text{LiBH}_4 + \text{Al}$, 277 °C [18]. A reduction of activation barrier can be responsible for the reduced dehydrogenation temperatures, as pointed out above. Another good point concerning all the studied materials is that the dehydrogenation is rapid, completed within 1 h, mainly during the heating period.

The effect of dehydrogenation pressure. It must be pointed out that this is the first report of dehydrogenation of $2\text{LiBH}_4 + \text{Al}$ /additive mixtures at non-vacuum pressures, i.e., at fuel cell compatible working pressures. Thus the possibility of using these mixtures has been demonstrated for disposable or non-rechargeable hydrogen storage applications as long as further re-hydrogenation can be proved. In general, our materials dehydrogenated at 3 bar presented a better hydrogen release quantity. Further research will be conducted to prove if re-hydrogenation is possible.

The effect of the additives. TiF_3 is a well-known additive in the hydrogen storage area, it is almost mandatory to try TiF_3 as an additive in hydrogen storage systems. Meanwhile, CeO_2 is not commonly used as an additive. CeO_2 has been anticipated to interact with hydrogen [25], and a revision of its effects as additive deserve attention. However, few examples have been published. Ceria could uptake small amounts of hydrogen below 391 °C [39]. Even more, Lin et al. [39] demonstrated an interfacial effect of $\text{CeH}_{2.73}/\text{CeO}_2$ functioning as “hydrogen pump” and reducing the hydrogen desorption temperature of $\text{MgH}_2\text{--Mg}_2\text{NiH}_4\text{--CeH}_{2.73}/\text{CeO}_2$. In that work [39], $\text{CeH}_{2.73}$ and CeO_2 were formed during successive hydrogenation and oxidation reactions. LiBH_4 or $\text{LiBH}_4 + 1/2\text{MgH}_2$ were mixed with CeCl_3 , CeF_3 , or CeH_2 to improve the hydrogenation/dehydrogenation kinetics, reversibility, or to reduce dehydrogenation temperature [40–44]. In the present work, CeO_2 demonstrated its effectiveness reducing the dehydrogenation temperature. The characterization of dehydrogenated materials by powder X-ray diffraction demonstrated the formation of CeB_6 . This boride has been observed after dehydrogenation of LiBH_4 or $\text{LiBH}_4 + 1/2\text{MgH}_2$ destabilized with CeCl_3 , CeF_3 , or CeH_2 [40–44]. On the other hand, X-ray diffraction did not show additional formation of Li or Al-oxides by liberation of the oxygen of CeO_2 . The expected formation of oxides is low: for example, a mass balance indicates that if all the oxygen of CeO_2 forms Li_2O , the lithium oxide would be 1.7 wt %. To conclude this part, CeO_2 additive was effective in reducing the dehydrogenation temperature and producing good hydrogen release.

4. Materials and Methods

4.1. Sample Preparation

All reactives were purchased from Sigma-Aldrich and used without further purification. The Al was granular, with a particle size roughly of 1 mm and 99.7% purity. The LiBH_4 purity was $\geq 95\%$, meanwhile, the purity of TiF_3 and CeO_2 were 99% and 99.995% respectively. The molar ratio of LiBH_4 and Al was 2:1. The amount of the additive in each sample was 5 wt %. The mixtures of $2\text{LiBH}_4 + \text{Al} +$ additives were produced by mechanical milling. The milling was performed in batches of 1 gram of mixture as needed for performing reactions or characterization. The milling was performed in a planetary mill (Across-International) with a rotation of the main plate of 2400 rpm. The milling vials were machined in stainless steel 316 L with an internal volume of 100 mL, with bolted lids. The milling balls were of yttrium-stabilized zirconium oxide (1 cm diameter). The powder to ball ratio was 1:15. The total milling time was 5 h divided into periods of 1 h milling and 10 min resting. In each cycle of milling-pause, the rotation direction of the planetary mill was inverted. The handling and storage of materials were performed inside a glove box filled with welding grade argon.

4.2. Characterization of the Ball-Milled and Dehydrogenated Materials

Scanning electron microscopy (SEM) images were obtained in a JSM-IT300 microscope (JEOL, Tokio, Japan). Samples were dispersed on carbon tape over a Cu sample holder. The SEM samples

were prepared inside the argon glove box and transferred to the microscope by means of a glove bag to avoid oxidation; however, slight oxidation could have been possible. SEM images were obtained by backscattered or secondary electrons and 10 kV or 20 kV of acceleration voltage, accordingly to each sample characteristics.

Powder X-ray diffraction (PXRD) characterization was performed in a BrukerB8 diffractometer (Cu $K\alpha = 1.540598 \text{ \AA}$, Bruker AXS, Karlsruhe, Germany). The powders of as-milled and dehydrogenated materials were compacted in a dedicated sample-holder, then they were covered with a Kapton foil for protection against ambient oxygen and moisture. Data processing and phase identification were performed with Diffract Suite Eva (Version 4.2.1.10, Bruker AXS, Karlsruhe, Germany, 2016) or MAUD software (Version 2.55, Trento University, Trento, Italy, 2015). ICSD (Inorganic Crystal Structure Database, Karlsruhe) or COD (Crystallography Open Database) databases were used for phase identification.

Fourier transformed infrared spectroscopy characterization was performed in a Varian 640-IR, FT-IR Spectrometer (Agilent Technologies, Santa Clara, CA, USA). The studied materials were compacted in KBr pellets. The KBr was purchased from Sigma-Aldrich and dried just before pellet preparation. About 2.5 mg of each material was dispersed in 50 mg of dry KBr. FT-IR data was collected in attenuated total reflection (ATR) mode.

X-ray photoelectron spectroscopy analyses were performed only on the as-milled materials. XPS experiments were accomplished in an ultra-high vacuum (UHV) system Scanning XPS microprobe PHI 5000 Versa Probe II (Physical Electronics, Minneapolis, United States of America), with an Al $K\alpha$ X-ray source (photon energy of 1486.6 eV) monochromatic at 25.4 W, and an multichannel detector. The surface of the samples was etched for 5 min with 1 kV Ar^+ at $55.56 \text{ nA}\cdot\text{mm}^{-2}$. The XPS spectra were obtained at 45° to the normal surface in the constant pass energy mode, $E_0 = 117.40$ and 11.75 eV for survey surface and high-resolution narrow scan, respectively. The peak positions were referenced to the background silver $3d_{5/2}$ photo-peak at 368.2 eV, having an FWHM of 0.56 eV, and C 1s hydrocarbon groups at 285.0 eV, Au $4f_{7/2}$ in 84.0 eV central peak core level position. XPS characterization was performed on the as-milled materials and raw materials NaBH_4 and Al as necessary. Powder samples were compacted in an adequate sample holder and transferred to the equipment by means of a glove bag.

4.3. Dehydrogenation Reaction

Dehydrogenations of $2\text{LiBH}_4 + \text{Al} + \text{additive materials}$ were performed in a Sievert's-type reactor. This reactor was designated and constructed by the research group. It consists basically of twins of a sample holder and a reference holder, a well-known-volume reservoir of H_2 for sample and a well-known-volume reservoir of H_2 for reference, high precision pressure transducers for sample and reference, and delicate control of the reservoirs, reference-holder and sample-holder temperatures. The registered temperatures and pressures versus time were converted to hydrogen release in wt % with the following formula [45]:

$$\text{wt \%}(\text{H}_2) = 100 \times \frac{M(\text{H}_2) \times \Delta p \times V_{\text{sample}}}{m \times R \times T_{\text{sample}} \times Z_{\text{fact}}} + 100 \times \frac{M(\text{H}_2) \times \Delta p \times V_{\text{reservoir}}}{m \times R \times T_{\text{reservoir}} \times Z_{\text{fact}}}, \quad (2)$$

where $M(\text{H}_2)$ is the hydrogen molar mass ($2.01588 \text{ g}\cdot\text{mol}^{-1}$). $\Delta p = \Delta p_{\text{sample}} - \Delta p_{\text{reference}}$ is in bar, where Δp_{sample} and $\Delta p_{\text{reference}}$ mean the actual pressure minus the initial pressure of sample and reference. At zero-time both sample and reference initial pressures are equal. This performs as a differential pressure transducer and helps reducing small (1×10^{-3} bar) variations of the pressures caused by thermal effects. The V and T are the volume and temperature of the reservoir and sample holder, in cm^3 and Kelvin degrees respectively; m is the sample mass in g; R is the gas constant ($83.14459 \text{ cm}^3\cdot\text{bar}\cdot\text{K}^{-1}\cdot\text{mol}^{-1}$) and, Z_{fact} is the hydrogen compressibility factor [46,47]. It is necessary to

mention that the sample holder and reference holder volume account for less than 1% of the reservoirs volume, meeting the appropriate conditions for hydrogen sorption/desorption and Sieverts law.

Samples were transferred to/from the Sieverts-type reactor without oxygen contact by means of a closing valve at the sample holder. Dehydrogenations were performed by a temperature-controlled process. The dehydrogenation initial pressure was fixed manually at 3 or 5 bar, the reservoir temperature was fixed at 40 °C. The sample temperature was raised from room temperature to 350 °C or 400 °C with a heating rate of 5 or 6 °C/min. The total dehydrogenation time was 3 h. Then, the system was cooled down and the remaining hydrogen was released. The dehydrogenation reaction was marked by a significant and sudden increase of the registered pressure beyond the temperature effects. The gases, hydrogen and argon, used during the dehydrogenation experiments were of chromatographic and high purity grade.

5. Conclusions

The 2LiBH₄ + Al/additives mixtures were prepared by ball milling. The milling conditions were optimized for the integration of Al and preservation of 2LiBH₄. The use of additives TiF₃ and CeO₂ produced different morphologies with as-milled materials. The studied materials presented a significant reduction of the dehydrogenation temperature that can be related to the surface-oxidation. The surface oxidation was the result of the use of welding-grade argon. The dehydrogenation reactions were observed to take place in two main steps, with onsets at 100 °C and 200–300 °C. The maximum released hydrogen was 9.3 wt % in the 2LiBH₄ + Al/TiF₃ material, and 7.9 wt % in the 2LiBH₄ + Al/CeO₂ material. Formation of CeB₆ after dehydrogenation of 2LiBH₄ + Al/CeO₂ was confirmed.

Supplementary Materials: The following are available online at www.mdpi.com/2304-6740/5/4/82/s1, Figure S1: SEM image of LiBH₄ (not ball-milled), Figure S2: SEM image of Al (not ball-milled), Figure S3: SEM of as-milled 2LiBH₄ + Al material, Figure S4: SEM of as-milled 2LiBH₄ + Al/TiF₃ material, Figure S5: SEM of as-milled 2LiBH₄ + Al/CeO₂ material, Figure S6: FT-IR of the as-milled 2LiBH₄ + Al, 2LiBH₄ + Al/TiF₃ and 2LiBH₄/CeO₂, Figure S7: Al 1s XPS of the as-milled 2LiBH₄ + Al, 2LiBH₄ + Al/TiF₃ and 2LiBH₄/CeO₂, Figure S8: SEM of dehydrogenated 2LiBH₄ + Al at 5 bar 400 °C, Figure S9: SEM of dehydrogenated 2LiBH₄ + Al at 3 bar 400 °C, Figure S10: SEM and EDS of dehydrogenated 2LiBH₄ + Al/TiF₃ at 5 bar 400 °C, Figure S11: SEM and EDS of dehydrogenated 2LiBH₄ + Al/TiF₃ at 3 bar 400 °C, Figure S12: SEM of dehydrogenated 2LiBH₄ + Al/CeO₂ DHH 5 bar 400 °C, Figure S13: SEM of dehydrogenated 2LiBH₄ + Al/CeO₂ DHH 3 bar 400 °C, Figure S14: Dehydrogenation of 2LiBH₄ + Al/CeO₂ (3 bar and 5 bar, 350 °C), Figure S15: SEM of dehydrogenated 2LiBH₄ + Al/CeO₂ DHH 5 bar 350 °C, Figure S16: EDS of dehydrogenated 2LiBH₄ + Al/CeO₂ DHH 5 bar 350 °C.

Acknowledgments: The present work was supported by SENER-CONACyT Project 215362 “Investigación en mezclas reactivas de hidruro: nanomateriales para almacenamiento de hidrógeno como vector energético”. Authors want to thank Omar Solorza-Feria and CINVESTAV-DF for facilitating FT-IR characterization. Authors would also like to thank Orlando Hernández for SEM characterization. XRD was performed at Universidad Autónoma Metropolitana-Iztapalapa, we thank Federico González García. Authors would like to thank Sandra Rodil and Lázaro Huerta Arcos for XPS characterization at IIM-UNAM.

Author Contributions: The findings in this manuscript are part of Juan Luis Carrillo-Bucio master’s degree work. Juan Rogelio Tena-García performed the XRD experiments and interpretation. The manuscript was written with contributions of all authors. All authors have given approval to the final version of the manuscript.

Conflicts of Interest: The authors declare no conflict of interest.

References

1. Züttel, A.; Wenger, P.; Rentsch, S.; Sudan, P.; Mauron, P.; Emmenegger, C. LiBH₄ a new hydrogen storage material. *J. Power Sources* **2003**, *118*, 1–7. [[CrossRef](#)]
2. Lee, J.Y.; Ravnsbæk, D.; Lee, Y.S.; Kim, Y.; Cerenius, Y.; Shim, H.J.; Jensen, T.R.; Hur, N.H.; Cho, Y.W. Decomposition reactions and reversibility of the LiBH₄-Ca(BH₄)₂ composite. *J. Phys. Chem. C* **2009**, *113*, 15080–15086. [[CrossRef](#)]
3. Liu, Y.; Reed, D.; Paterakis, C.; Contreras Vasquez, L.; Baricco, M.; Book, D. Study of the decomposition of a 0.62LiBH₄-0.38NaBH₄ mixture. *Int. J. Hydrog. Energy* **2017**, *42*, 22480–22488. [[CrossRef](#)]

4. Gil-Bardají, E.; Zhao-Karger, Z.; Boucharat, N.; Nale, A.; van Setten, M.J.; Lohstroh, W.; Reohm, E.; Catti, M.; Fichtner, M. $\text{LiBH}_4\text{-Mg}(\text{BH}_4)_2$: A physical mixture of metal borohydrides as hydrogen storage material. *J. Phys. Chem. C* **2011**, *115*, 6095–6101. [[CrossRef](#)]
5. Aoki, M.; Miwa, K.; Noritake, T.; Kitahara, G.; Nakamori, Y.; Orimo, S.; Towata, S. Destabilization of LiBH_4 by mixing with LiNH_2 . *Appl. Phys. A* **2005**, *80*, 1409–1412. [[CrossRef](#)]
6. Mao, J.F.; Guo, Z.P.; Liua, H.K.; Yu, X.B. Reversible hydrogen storage in titanium-catalyzed $\text{LiAlH}_4\text{-LiBH}_4$ system. *J. Alloys Compd.* **2009**, *487*, 434–438. [[CrossRef](#)]
7. Shi, Q.; Yu, X.; Feidenhans, R.; Vegge, T. Destabilized $\text{LiBH}_4\text{-NaAlH}_4$ mixtures doped with titanium based catalysts materials research. *J. Phys. Chem. C* **2008**, *112*, 18244–18248. [[CrossRef](#)]
8. Vajo, J.J.; Skeith, S.L.; Mertens, F. Reversible storage of hydrogen in destabilized LiBH_4 . *J. Phys. Chem. B* **2005**, *109*, 3719–3722. [[CrossRef](#)] [[PubMed](#)]
9. Barkhordarian, G.; Klassen, T.; Dornheim, M.; Bormann, R. Unexpected kinetic effect of MgB_2 in reactive hydride composites containing complex borohydrides. *J. Alloys Compd.* **2007**, *440*, L18–L21. [[CrossRef](#)]
10. Bösenberg, U.; Doppiu, S.; Mosegaard, L.; Barkhordarian, G.; Eigen, N.; Borgschulte, A.; Jensen, T.R.; Cerenius, Y.; Gutfleisch, O.; Klassen, T.; et al. Hydrogen sorption properties of $\text{MgH}_2\text{-LiBH}_4$ composites. *Acta Mater.* **2007**, *55*, 3951–3958. [[CrossRef](#)]
11. Pinkerton, F.E.; Meyer, M.S. Reversible hydrogen storage in the lithium borohydride—Calcium hydride coupled system. *J. Alloys Compd.* **2008**, *464*, L1–L4. [[CrossRef](#)]
12. Yang, J.; Sudik, A.; Wolverton, C. Destabilizing LiBH_4 with a Metal ($M = \text{Mg, Al, Ti, V, Cr, or Sc}$) or Metal Hydride ($\text{MH}_2 = \text{MgH}_2, \text{TiH}_2, \text{or CaH}_2$). *J. Phys. Chem. C* **2007**, *111*, 19134–19140. [[CrossRef](#)]
13. Li, Y.; Li, P.; Qu, X. Investigation on $\text{LiBH}_4\text{-CaH}_2$ composite and its potential for thermal energy storage. *Sci. Rep.* **2017**, *7*, 41754–41758. [[CrossRef](#)] [[PubMed](#)]
14. Arnbjerg, L.M.; Ravnsbæk, D.B.; Filinchuk, Y.; Vang, R.T.; Cerenius, Y.; Besenbacher, F.; Jørgensen, J.E.; Jakobsen, H.J.; Jensen, T.R. Structure and dynamics for $\text{LiBH}_4\text{-LiCl}$ solid solutions. *Chem. Mater.* **2009**, *21*, 5772–5782. [[CrossRef](#)]
15. Yu, X.B.; Grant, D.M.; Walker, G.S. Dehydrogenation of LiBH_4 destabilized with various oxides. *J. Phys. Chem. C* **2009**, *113*, 17945–17949. [[CrossRef](#)]
16. Lee, H.S.; Hwang, S.J.; To, M.; Lee, Y.S.; Whan Cho, Y. Discovery of fluidic LiBH_4 on scaffold surfaces and its application for fast co-confinement of $\text{LiBH}_4\text{-Ca}(\text{BH}_4)_2$ into mesopores. *J. Phys. Chem. C* **2015**, *119*, 9025–9035. [[CrossRef](#)]
17. Hansen, B.R.S.; Ravnsbæk, D.B.; Reed, D.; Book, D.; Gundlach, C.; Skibsted, J.; Jensen, T.R. Hydrogen storage capacity loss in a $\text{LiBH}_4\text{-Al}$ composite. *J. Phys. Chem. C* **2013**, *117*, 7423–7432. [[CrossRef](#)]
18. Siegel, D.J.; Wolverton, C.; Ozoliņš, V. Thermodynamic guidelines for the prediction of hydrogen storage reactions and their application to destabilized hydride mixtures. *Phys. Rev. B* **2007**, *76*, 134102–134106. [[CrossRef](#)]
19. Zhang, Y.; Tian, Q.; Zhang, J.; Liu, S.S.; Sun, L.X. The dehydrogenation reactions and kinetics of $2\text{LiBH}_4\text{-Al}$ composite. *J. Phys. Chem. C* **2009**, *113*, 18424–18430. [[CrossRef](#)]
20. Kang, X.D.; Wang, P.; Ma, L.P.; Cheng, H.M. Reversible hydrogen storage in LiBH_4 destabilized by milling with Al. *Appl. Phys. A* **2007**, *89*, 963–966. [[CrossRef](#)]
21. Ravnsbæk, D.B.; Jensen, T.R. Mechanism for reversible hydrogen storage in $\text{LiBH}_4\text{-Al}$. *J. Appl. Phys.* **2012**, *111*, 112621–112628. [[CrossRef](#)]
22. Bosenberg, U.; Ravnsbæk, D.B.; Hagemann, H.; D’Anna, V.; Bonatto-Minella, C.; Pistidda, C.; van Beek, W.; Jensen, T.R.; Bormann, R.; Dornheim, M. Pressure and temperature influence on the desorption pathway of the $\text{LiBH}_4\text{-MgH}_2$ composite system. *J. Phys. Chem. C* **2010**, *114*, 15212–15217. [[CrossRef](#)]
23. Saldan, I.; Llamas-Jansa, I.; Hino, S.; Frommen, C.; Hauback, B.C. Synthesis and thermal decomposition of $\text{Mg}(\text{BH}_4)_2\text{-TMO}$ ($\text{TMO} = \text{TiO}_2; \text{ZrO}_2; \text{Nb}_2\text{O}_5; \text{MoO}_3$) composites. *IOP Conf. Ser. Mater. Sci. Eng.* **2015**, *77*, 012041–012047. [[CrossRef](#)]
24. Saldan, I.; Frommen, C.; Llamas-Jansa, I.; Kalantzopoulos, G.N.; Hino, S.; Arstad, B.; Heyn, R.; Zavorotynska, O.; Deledda, S.; Sørby, M.H.; et al. Hydrogen storage properties of $\gamma\text{-Mg}(\text{BH}_4)_2$ modified by MoO_3 and TiO_2 . *Int. J. Hydrog. Energy* **2015**, *40*, 12286–12293. [[CrossRef](#)]
25. Sohlberg, K.; Pantelides, S.T.; Pennycook, S.J. Interactions of hydrogen with CeO_2 . *J. Am. Chem. Soc.* **2001**, *123*, 6609–6611. [[CrossRef](#)] [[PubMed](#)]
26. Suárez-Alcántara, K.; Palacios-Lazcano, A.F.; Funatsu, T.; Cabañas-Moreno, J.G. Hydriding and dehydriding in air-exposed Mg-Fe powder mixtures. *Int. J. Hydrog. Energy* **2016**, *41*, 23380–23387. [[CrossRef](#)]

27. Kato, S.; Biemann, M.; Borgschulte, A.; Zakaznova-Herzog, V.; Remhof, A.; Orimo, S.I.; Züttel, A. Effect of the surface oxidation of LiBH_4 on the hydrogen desorption mechanism. *Phys. Chem. Chem. Phys.* **2010**, *12*, 10950–10955. [CrossRef] [PubMed]
28. JANAF Thermochemical Tables. Available online: <http://kinetics.nist.gov/janaf/> (accessed on 15 July 2017).
29. Fang, Z.Z.; Ma, L.P.; Kang, D.; Wang, P.J.; Wang, P.; Cheng, H.M. In situ formation and rapid decomposition of $\text{Ti}(\text{BH}_4)_3$ by mechanical milling LiBH_4 with TiF_3 . *Appl. Phys. Lett.* **2009**, *94*. [CrossRef]
30. D'Anna, V.; Spyratou, A.; Sharma, M.; Hagemann, H. FT-IR spectra of inorganic borohydrides. *Spectrochim. Acta Part A Mol. Biomol. Spectrosc.* **2014**, *128*, 902–906. [CrossRef] [PubMed]
31. Xiong, Z.; Cao, L.; Wang, J.; Mao, J. Hydrolysis behavior of LiBH_4 films. *J. Alloys Compd.* **2017**, *698*, 495–500. [CrossRef]
32. Haerberle, J.; Henkel, K.; Gargouri, H.; Naumann, F.; Gruska, B.; Arens, M.; Tallarida, M.; Schmeißer, D. Ellipsometry and XPS comparative studies of thermal and plasma enhanced atomic layer deposited Al_2O_3 -films. *J. Nanotechnol.* **2013**, *4*, 732–742. [CrossRef] [PubMed]
33. Van den Brand, J.; Sloof, W.G.; Terryn, H.; de Wit, J.H.W. Correlation between hydroxyl fraction and O/Al atomic ratio as determined from XPS spectra of aluminum oxide layers. *Surf. Interface Anal.* **2004**, *36*, 81–88. [CrossRef]
34. Ramezani, M.; Neitzert, T. Mechanical milling of aluminum powder using planetary ball milling process. *J. Achiev. Mater. Manuf. Eng.* **2012**, *55*, 790–798.
35. Kang, J.K.; Kim, S.Y.; Han, Y.S.; Muller, R.P.; Goddard, W.A., III. A candidate LiBH_4 for hydrogen storage: Crystals structures and reaction mechanisms of intermediate phases. *Appl. Phys. Lett.* **2005**, *87*. [CrossRef]
36. Züttel, A.; Rentsch, S.; Fischer, P.; Wenger, P.; Sudan, P.; Mauron, P.; Emmenegger, C. Hydrogen storage properties of LiBH_4 . *J. Alloys Compd.* **2003**, *356–357*, 515–520. [CrossRef]
37. Kim, K.B.; Shim, J.H.; Park, S.H.; Choi, I.S.; Oh, K.H.; Cho, Y.W. Dehydrogenation reaction pathway of the LiBH_4 - MgH_2 composite under various pressure conditions. *J. Phys. Chem. C* **2015**, *119*, 9714–9720. [CrossRef]
38. Friedrichs, O.; Kim, J.W.; Remhof, A.; Buchter, F.; Borgschulte, A.; Wallacher, D.; Cho, Y.W.; Fichtner, M.; Oh, K.H.; Züttel, A. The effect of Al on the hydrogen sorption mechanism of LiBH_4 . *Phys. Chem. Chem. Phys.* **2009**, *11*, 1515–1520. [CrossRef] [PubMed]
39. Lin, H.J.; Tang, J.J.; Yu, Q.; Wang, H.; Ouyang, L.Z.; Zhao, Y.J.; Liu, J.W.; Wang, W.H.; Zu, M. Symbiotic $\text{CeH}_{2.73}/\text{CeO}_2$ catalyst: A novel hydrogen pump. *Nano Energy* **2014**, *9*, 80–87. [CrossRef]
40. Gennari, F.C.; Fernández Albanesi, L.; Puzskiel, J.A.; Arneodo Larochette, P. Reversible hydrogen storage from $6\text{LiBH}_4\text{-MCl}_3$ ($\text{M} = \text{Ce}, \text{Gd}$) composites by in-situ formation of MH_2 . *Int. J. Hydrog. Energy* **2011**, *36*, 563–570. [CrossRef]
41. Liu, B.H.; Zhang, B.J.; Jiang, Y. Hydrogen storage performance of $\text{LiBH}_4 + 1/2\text{MgH}_2$ composites improved by Ce-based additives. *Int. J. Hydrog. Energy* **2011**, *36*, 5418–5424. [CrossRef]
42. Jin, S.A.; Lee, Y.S.; Shim, J.H.; Cho, Y.W. Reversible hydrogen storage in $\text{LiBH}_4\text{-MH}_2$ ($\text{M} = \text{Ce}, \text{Ca}$) composites. *J. Phys. Chem. C* **2008**, *112*, 9520–9524. [CrossRef]
43. Gennari, F.C. Destabilization of LiBH_4 by MH_2 ($\text{M} = \text{Ce}, \text{La}$) for hydrogen storage: Nanostructural effects on the hydrogen sorption kinetics. *Int. J. Hydrog. Energy* **2011**, *36*, 15231–15238. [CrossRef]
44. Zhang, B.J.; Liu, B.H.; Li, Z.P. Destabilization of LiBH_4 by $(\text{Ce}, \text{La})(\text{Cl}, \text{F})_3$ for hydrogen storage. *J. Alloys Compd.* **2011**, *509*, 751–757. [CrossRef]
45. Peschke, M. Wasserstoffspeicherung in Reaktiven Hydrid-Kompositen Einfluss von fluorbasierten Additiven auf das Sorptionsverhalten des $\text{MgB}_2\text{-LiH}$ -Systems. Diplomarbeit (Undergraduate Thesis), GKSS-Forschungszentrum Geesthacht GmbH Helmut-Schmidt-Universität/Universität der Bundeswehr, Hamburg, Germany, April 2009.
46. Züttel, A.; Borgschulte, A.; Schlapbach, L.; Chorkendorf, I.; Suda, S. Properties of hydrogen. In *Hydrogen as A Future Energy Carrier*; Züttel, A., Borgschulte, A., Schlapbach, L., Eds.; John Wiley & Sons: Weinheim, Germany, 2008; pp. 71–94. ISBN 978-3-527-30817-0.
47. Hemmes, H.; Driessen, A.; Driessen, R. Thermodynamic properties of hydrogen at pressures up to 1 Mbar and Temperatures between 100 and 1000 K. *J. Phys. C Solid State Phys.* **1986**, *19*, 3571–3585. [CrossRef]

